Eur. Phys. J. B (2013) 86: 201
DOI: 10.1140/epjb/e2013-40071-x

THE EUROPEAN PHYSICAL JOURNAL B

Regular Article

# Phonon excitations and magnetoelectric coupling in multiferroic $RMn_2O_5$

Safa Golrokh Bahoosh[1], Julia M. Wesselinowa[2], and Steffen Trimper[3,a]

[1] Max Planck Institute of Microstructure Physics, 06120 Halle, Germany
[2] Department of Physics, University of Sofia, 1164 Sofia, Bulgaria
[3] Institute of Physics, Martin-Luther-University, 06120 Halle, Germany

Received 28 January 2013 / Received in final form 4 March 2013
Published online 2nd May 2013 – © EDP Sciences, Società Italiana di Fisica, Springer-Verlag 2013

**Abstract.** Multiferroic rare-earth manganites are theoretically studied by focusing on the coupling to the lattice degrees of freedom. We demonstrate analytically that the phonon excitations in the multiferroic phase are strongly affected by the magnetoelectric coupling, the spin-phonon interaction and the anharmonic phonon-phonon interaction. Based on a microscopic model, the temperature dependence of the phonon dispersion relation is analyzed. It offers an anomaly at both the ferroelectric and the magnetic transition indicating the mutual coupling between multiferroic orders and lattice distortions. Depending on the sign of the spin-phonon coupling the phonon modes become softer or harder in accordance with experimental observations. We show that the phonon spectrum can be also controlled by an external magnetic field. The phonon energy is enhanced by increasing that field. The applied Green's function technique allows the calculation of the macroscopic magnetization depending on both the phonon-phonon and the spin-phonon couplings.

## 1 Introduction

Recently, a large class of manganese oxides as $R\mathrm{MnO_3}$ and $R\mathrm{Mn_2O_5}$, with rare earth $R$ = Y, Tb, Dy, etc. has been discovered to reveal a strong magnetoelectric coupling (ME) [1]. The material offers multiferroic properties characterized by the coexistence of magnetic and ferroelectric orders. The ME coupling leads to various novel physical effects, such as the colossal magneto dielectric effects [2] and magnetospin-flop effects [3]. As reported in reference [4] the ME coupling in $\mathrm{TbMn_2O_5}$ is so strong that the electric polarization can be reversed by applying a magnetic field. The remarkable ME effects in these materials have attracted a great deal of interest due to the fascinating physical properties and the potential applications in novel multi-functional ME devices. Regardless the innovative aspects, the underlying detailed mechanism of the multiferroics is under a permanent debate, for a recent review see [5–7]. Since in the past phonons and their coupling with other degrees of freedom have played a crucial role in understanding classic ferroelectrics, one should expect that they have a great impact on magnetoelectric multiferroics. Recent investigations using Raman and infrared (IR) spectroscopy, by transmittance and reflectance measurements, have demonstrated the importance of phonon effects in multiferroics. There is an experimental evidence for a strong spin-phonon coupling in $R\mathrm{Mn_2O_5}$ [8,9]. The experimental results show pronounced phonon anomalies around the magnetic and electric phase transition temperatures [10–15]. These anomalies are attributed to the multiferroic character of the materials. Raman phonons in $R\mathrm{MnO_3}$ orthorhombic and hexagonal manganites have been studied in reference [16] as a function of the rare-earth ion and the temperature. The sign and the magnitude of such anomalous phonon shifts seem to be correlated with the ionic radius of the multiferroic $R\mathrm{Mn_2O_5}$ [11]. So the phonon excitation becomes a soft mode in case that $R$ is Bi and is hardening if the rare-earth part is Dy. An intermediate behavior is observed for Eu. Based on the temperature dependence of the far-IR transmission spectra of multiferroic $\mathrm{YMn_2O_5}$ and $\mathrm{TbMn_2O_5}$ single crystals, the occurrence of electromagnons was reported in $R\mathrm{Mn_2O_5}$ compounds in reference [17]. The phonon energy and its damping are different for diverse compounds. So varying selection rules for electromagnons in $R\mathrm{Mn_2O_5}$ and $R\mathrm{MnO_3}$ suggest different magneto-elastic coupling mechanisms in the multiferroic systems. Molecular-spin dynamics study of electromagnons in $R\mathrm{Mn_2O_5}$ are discussed in reference [18]. The so-called shell model lattice dynamic calculations are proposed in reference [19] for $R\mathrm{Mn_2O_5}$ ($R$ = Ho, Dy) materials. Here spin-phonon couplings have been taken into account. Theoretically the influence of phonons is studied in reference [20]. The exchange-striction induces a biquadratic interaction

[a] e-mail: steffen.trimper@physik.uni-halle.de

between spins and transverse phonons. Furthermore, the Dzyaloshinskii-Moriya interaction is considered in references [20,21]. More recently, the spin-phonon coupling in multiferroic Mn compounds were analyzed in a classical spin-model [22]. Using a microscopic model in reference [23] the properties of thin films composed of multiferroic material have been studied.

The new aspect focused on in the present paper is the calculation of the phonon spectrum within a microscopic model for $R\mathrm{Mn_2O_5}$. Here the magnetic subsystem is described by a Heisenberg spin Hamiltonian with two competing coupling parameters which give rise to frustration. The magnetic subsystem offers a phase transition at $T_N$. In modeling the ferroelectric behavior we have to take into account the improper nature of ferroelectricity. To that aim we concentrate the analysis of the ferroelectric subsystem on a parameter range where the polarization is induced by the magnetoelectric coupling exclusively. With other words the polarization is zero for $T \leq T_N$. Lowering the temperature further the magnetoelectric (ME) coupling leads to a finite polarization at $T_C$, where $T_C < T_N$. Due to the complexity of the manganites the ferroelectric behavior is described within our analytical approach by both order-disorder and displacive type aspects. The order-disorder properties are characterized by pseudo-spins in the frame of an Ising model in a transverse field [24], while the displacive behavior is characterized by lattice distortions. Based on a tractable analytical model we show that the magnetoelectric coupling, the spin-phonon interaction as well as the anharmonic phonon-phonon interaction contribute to the phonon excitations in a significant manner. So the temperature dependent phonon spectrum exhibits an anomaly at the ferroelectric and the magnetic phase transitions. The related excitation is obtained applying temperature dependent Green's function methods. The methods allows also the computation of the macroscopic magnetization. Furthermore, we demonstrate that the phonon mode can be also controlled by an external magnetic field. The analytical finding is compared with experimental results.

## 2 The model

### 2.1 Hamiltonian

The known mechanisms of the spin-polarization coupling can be categorized in two different types. One of them is based on the inverse Dyzaloshinskii-Moriya interaction, where the local dipole moment, denoted by $u_{ij}$, couples to two canted spins $S_i$ and $S_j$ in the form proportional to $u_{ij} \cdot \hat{e}_{ij} \times (\vec{S}_i \times \vec{S}_j)$. The unit vector $\hat{e}_{ij}$ connects the centers of the magnetic ions at lattice sites $i$ and $j$. The microscopic origin of such coupling was investigated in several papers such as [25,26]. The properties of a whole class of multiferroic materials as $R\mathrm{MnO_3}$ can be understood on the basis of this coupling. The second type of coupling arises from exchange-striction, wherein the magnetic ions are assumed to be influenced directly by the exchange interaction giving rise to a coupling proportional to $\hat{e}_{ij} \cdot (u_i - u_j)(\vec{S}_i \cdot \vec{S}_j)$ [27–29]. Because such spin-lattice coupling is believed to be relevant for $R\mathrm{Mn_2O_5}$ we follow the line of the second kind of coupling.

As already emphasized [20] a more realistic model should include both aspects, namely a frustrated magnetic system as well as symmetric exchange-striction. The ME coupling induces the polarization at temperature $T_C$ which is lower than the magnetic transition temperature $T_N$. Within an analytical approach one has to incorporate the ferroelectric behavior in the total Hamiltonian of the system. In our model that subsystem is characterized by a displacive type interaction and an order-disorder behavior. Whereas the order-disorder type interaction is simply described by an Ising model in a transverse field [24] the displacive behavior is written in terms of lattice distortions. The Hamiltonian reads

$$H = H_\mathrm{m} + H_\mathrm{f} + H_\mathrm{mf}. \tag{1}$$

The magnetic part $H_m$ is expressed by the Heisenberg spin Hamiltonian

$$H_\mathrm{m} = -\frac{1}{2}\sum_{ij} J_{ij}\vec{S}_i \cdot \vec{S}_j + \frac{1}{2}\sum_{\langle ij\rangle} \tilde{J}_{ij}\vec{S}_i \cdot \vec{S}_j - h\sum_i S_i^z. \tag{2}$$

Here, $h = g\mu_B B$ is the external magnetic field. The Hamiltonian $H_\mathrm{m}$ consists of the isotropic Heisenberg exchange interaction with nearest neighbor ferromagnetic interaction $J > 0$, denoted as $ij$, and next nearest neighbor antiferromagnetic coupling $\tilde{J} > 0$, indicated by $\langle ij\rangle$ in equation (2). Due to the mixed ferromagnetic and antiferromagnetic coupling the system exhibits frustration in case $\tilde{J} > J/4$ [30]. Let us make some remarks concerning the magnetic interaction. As pointed out in reference [31], compare also [32], the magnetic excitations in the multiferroic material are more different. Within a numerical simulation the authors have identified five different exchange coupling parameters appearing in the Heisenberg spin Hamiltonian. Following [29], the exchange interactions between neighboring $Mn^{3+}$ and $Mn^{4+}$ ions are all antiferromagnetic. As a result, magnetic frustration must exist in the smallest closed loop of Mn spins consisting of five magnetic ions. So, zigzag chains of frustrated spins exist in a direction parallel to the a axis as it is illustrated in Figure 1a. In the framework of an analytical calculation, it would be to complicated to formulate the situation by a Hamiltonian and solving the corresponding equations for such a sophisticated spin structure. Therefore, we have simplified the model as depicted in Figure 1b. It comprises the frustrated magnetic subsystem represented by equation (2). The two different couplings $J$ and $\tilde{J}$ in this equation reflect the competition between different magnetic orders which gives reason to frustration.

The ferroelectric subsystem $H_\mathrm{f}$ is characterized by lattice distortions describing the displacive type behavior and pseudospins within the Ising model in a transverse field

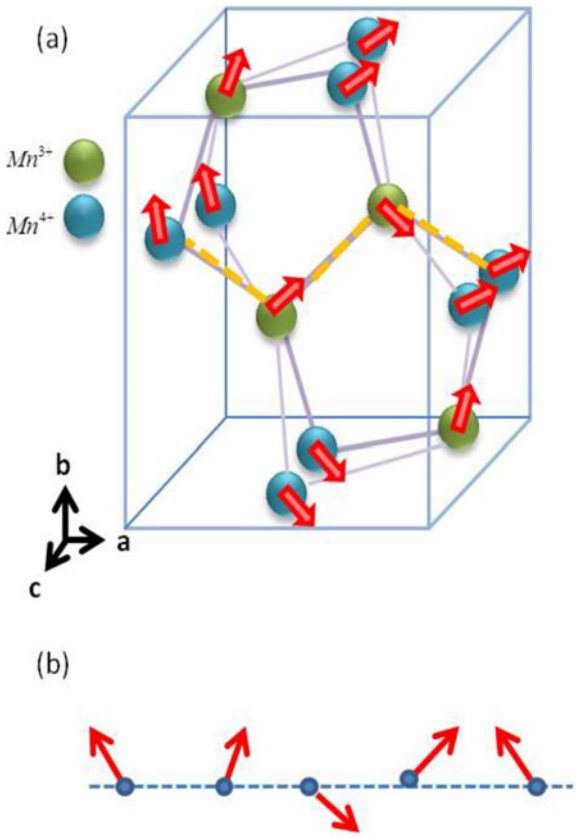



**Fig. 1.** (a) Mn-spin configuration in $RMn_2O_5$ structure showing frustration. (b) Typical sketch of a frustrated spin system with nearest neighbor ferromagnetic interaction and next nearest neighbor antiferromagnetic coupling.

reflecting the order-disorder behavior. Therefore $H_{\rm f}$ is

$$\begin{aligned} H_{\rm f} &= H_{\rm ph} + H_{\rm tim} \\ H_{\rm ph} &= \frac{1}{2}\sum_k \left(P_k P_{-k} + \omega^2_{(0)k} Q_k Q_{-k}\right) \\ &\quad + \frac{1}{3!}\sum_{kk_1} B(k,k_1) Q_k Q_{-k_1} Q_{k_1-k} \\ &\quad + \frac{1}{4!}\sum_{k,k_1k_2} A(k,k_1,k_2) Q_{k_1} Q_{k_2} Q_{-k-k_2} Q_{-k_1+k} \\ H_{\rm tim} &= -\frac{1}{2}\sum_{ij} J'_{ij} B^z_i B^z_j - 2\Omega \sum_i B^x_i . \end{aligned} \tag{3}$$

The first part of $H_{\rm ph}$ represents the harmonic part of the lattice distortions in terms of the normal coordinate $Q_k$, the momentum $P_k$ and the harmonic phonon frequency $\omega_{(0)k}$ of the lattice mode with wave vector $k$. The following terms describe the anharmonic interactions, where the third order coupling is given by $B(k,k_1)$ and the quartic one by $A(k,k_1,k_2)$. In terms of phonon creation and annihilation operators the normal coordinate and the momentum are expressed by:

$$\begin{aligned} Q_k &= (2\omega_{(0)k})^{-1/2}\left(a_k + a^\dagger_{-k}\right) \\ P_k &= i(\omega_{(0)k}/2)^{1/2}\left(a^\dagger_k - a_{-k}\right). \end{aligned} \tag{4}$$

The order-disorder part is represented by $H_{\rm tim}$ which is due to [24] written in terms of pseudo-spin operators $B^z$ and $B^x$. $J'_{ij}$ denotes the nearest neighbor pseudo-spin interaction and $\Omega$ is a frequency which allows a flip process between the two orientations of the moment $B^z$. The two orientations are given by the eigenvalues $\pm 1$ of the operator $B^z$. The ferroelectric subsystem is considered typically in a rotated frame according to

$$\begin{aligned} B^x_j &= \left(\frac{1}{2} - \rho_j\right)\sin\nu + \frac{1}{2}\left(b_j + b^\dagger_j\right)\cos\nu; \\ B^y_j &= \frac{i}{2}\left(b^\dagger_j - b_j\right); \\ B^z_j &= \left(\frac{1}{2} - \rho_j\right)\cos\nu - \left(b_j + b^\dagger_j\right)\sin\nu; \quad \rho_j = b^\dagger_j b_j. \end{aligned} \tag{5}$$

Here, $b$ and $b^\dagger$ are Pauli-operators which fulfill the commutator relation $[b_i, b^\dagger_j] = (1 - 2\rho_i)\,\delta_{ij}$. The angle $\nu$ is determined in such a manner that the polarization is zero provided the system is within the range $T_C \le T \le T_N$ and the magnetoelectric coupling is not relevant. This technical trick reflects the improper nature of the ferroelectricity. As demonstrated below the ferroelectricity is directly induced by the magnetoelectric coupling which will be introduced now.

The coupling between the ferroelectric and the magnetic subsystems includes a quadratic coupling in the magnetic order parameter and a linear one in the ferroelectric order parameter. Because the magnetic subsystem is expressed in terms of the spin-operator $\vec{S}$ and the ferroelectric one in terms of pseudo-spin operators $\vec{B}$, the relevant magnetoelectric coupling $H_{\rm mf}$ is given by

$$H_{\rm mf} = \sum_{ijl} K_{ijl} B^z_i \vec{S}_j \cdot \vec{S}_l. \tag{6}$$

The underlying physical mechanism of the coupling is that the cooperative alignment of magnetic moments at a certain temperature is the reason for the polarization. The ME coupling in equation (6) describes the direct influence of the magnetic order parameter on the secondary polar order parameter. However both subsystems are simultaneously influenced by lattice distortions. Hence the model has to be completed by spin-phonon interactions. Such a spin-phonon coupling had been already discussed within the pseudo-spin approach in reference [24]. As pointed out the main effect comes from the modulation of an internal crystal field. Following that approach and former studies for ferroelectric thin films in [33] as well as for multiferroic materials in reference [34], the pseudo-spin phonon coupling $H_{\rm fph}$ can be expressed in terms of normal displacement coordinates $Q$, compare equation (3). The total

interaction is written in the form

$$\begin{aligned} H_{\rm fph} &= -\sum_k F^{(f)}(k) Q_k B^z_{-k} \\ &\quad - \frac{1}{2}\sum_{kk_1} R^{(f)}(k,k_1) Q_k Q_{-k_1} B^z_{k_1-k} \\ H_{\rm mph} &= -\sum_k F^{(m)}(k) Q_k S^z_{-k} \\ &\quad - \frac{1}{2}\sum_{kk_1} R^{(m)}(k,k_1) Q_k Q_{-k_1} S^z_{k_1-k}. \end{aligned} \tag{7}$$

Here, the first term $H_{\rm fph}$ models the coupling between the ferroelectric order parameter and the phonons, while the second term $H_{\rm mph}$ is responsible for the coupling between phonons and magnetic spins. We are aware that higher order couplings, quadratic in spins or pseudo-spins, can be also taken into account. Such terms seem to be irrelevant in searching the occurrence of a polarization due to magnetic ordering. The complete Hamiltonian will be analyzed in the subsequent section using Green's functions.

### 2.2 Green's functions and excitation spectrum

A powerful technique to get the dispersion relation and related macroscopic quantities is the Green's function method at finite temperatures. For the magnetic subsystem let us define the Green's function due to [35]

$$\begin{aligned} G^m_q(t-t') &\equiv \left\langle\left\langle S^+_q(t); S^-_q(t')\right\rangle\right\rangle \\ &= -i\Theta(t-t')\left\langle\left[\, S^+_q(t)\,, S^-_q(t')\right]\right\rangle. \end{aligned} \tag{8}$$

Using the commutation relation and making a simple decoupling (RPA) it results

$$\begin{aligned} G^m_q(E) &= \frac{2\langle\sigma_M\rangle}{E - E^m(\vec{q})} \quad \text{with} \quad \mathrm{M} = \langle \mathrm{S^z}\rangle = \langle\sigma_{\mathrm{M}}\rangle \\ E^m(q) &= \langle S_z\rangle\left[J_0 - J_q + \tilde{J}_q - \tilde{J}_0 - K_0\cos\nu\left(\frac{1}{2} - \langle\rho\rangle\right)\right] \\ &\quad + F^{(m)}(0)\langle Q\rangle + R^{(m)}(0)\left\langle Q^2\right\rangle. \end{aligned} \tag{9}$$

Here $E^m$ is the spin-wave energy of the magnetic subsystem modified by the magnetoelectric coupling $K_0$ and the magnetic spin-phonon interaction $F^{(m)}$ and $R^{(m)}$. The magnetization $M$ is given by $M = \langle S^z\rangle = \langle\sigma_M\rangle$.

Because the ferroelectric subsystem is expressed in terms of pseudo-spin operators (see Eqs. (3), (5) and (7)), the related Green's function can be defined in a similar manner as for the magnetic system in equation (8). Different to the magnetic case the Green's function is a matrix abbreviated as $G^f_{lm}(t)$:

$$\begin{pmatrix} \langle\langle b_l; b^\dagger_m\rangle\rangle & \langle\langle b_l; b_m\rangle\rangle \\ \langle\langle b^\dagger_l; b^\dagger_m\rangle\rangle & \langle\langle b^\dagger_l; b_m\rangle\rangle \end{pmatrix} \equiv \begin{pmatrix} G^{f11}_{lm} & G^{f12}_{lm} \\ G^{f21}_{lm} & G^{f22}_{lm} \end{pmatrix}.$$

Here the notation is the same as in equation (8). A typical Green's function reads

$$\begin{aligned} G^{f11}_q &= \langle\sigma_P\rangle\left(\frac{\epsilon_q}{E - E_{\rm f}} - \frac{\epsilon'_q}{E + E_{\rm f}}\right) \\ E^f(q) &= \sqrt{(\varepsilon^{11}_q)^2 - (\varepsilon^{12}_q)^2}. \end{aligned} \tag{10}$$

The coefficients $\epsilon_q$, $\epsilon'_q$ as well as $\varepsilon^{11}_q$ and $\varepsilon^{11}_q$ can be found in Appendix A.

The phonon part is also described by a Green's function matrix denoted as $G^{\rm ph}_q(t)$. They are defined by:

$$\begin{pmatrix} \langle\langle a_q; a^\dagger_q\rangle\rangle & \langle\langle a_q; a_q\rangle\rangle \\ \langle\langle a^\dagger_q; a^\dagger_q\rangle\rangle & \langle\langle a^\dagger_q; a_q\rangle\rangle \end{pmatrix} \equiv \begin{pmatrix} G^{11}_q & G^{12}_q \\ G^{21}_q & G^{22}_q \end{pmatrix}. \tag{11}$$

These set of Green's functions fulfills the following equation of motion:

$$\begin{pmatrix} G^{11}_q & G^{12}_q \\ G^{21}_q & G^{22}_q \end{pmatrix} = \begin{pmatrix} 1 & 0 \\ 0 & -1 \end{pmatrix} + \begin{pmatrix} \varpi_q{}^{11} & \varpi_q{}^{12} \\ \varpi_q{}^{21} & \varpi_q{}^{22} \end{pmatrix}\begin{pmatrix} G^{11}_q & G^{12}_q \\ G^{21}_q & G^{22}_q \end{pmatrix}, \tag{12}$$

where the coefficients are also defined in Appendix B. The harmonic phonon frequency in equation (3) is modified by the different couplings. The renormalized phonon excitation energy is given by the poles of the related Green's function and reads

$$\begin{aligned} \omega^2_q = \omega^2_{(0)q} + 2\omega_{(0)q}\Bigg(&\bar{B}_q\langle Q\rangle + \frac{1}{2}\bar{A}_q\langle Q^2\rangle - \frac{1}{2}\bar{R}^{(m)}(q)\langle\sigma_M\rangle \\ &- \frac{1}{2}\bar{R}^{(f)}(q)\langle\sigma_P\rangle\cos\nu\Bigg). \end{aligned} \tag{13}$$

Let us stress that the renormalized phonon frequency in equation (13) is apart from the coupling parameters determined by the magnetization $\langle\sigma_M\rangle$ and the polarization $\langle\sigma_P\rangle$. Those macroscopic quantities like magnetization and polarization can be also found using Green's function. The analytical results will be discussed in the subsequent section.

## 3 Results and discussion

In the previous section we found an analytical expression for the phonon excitation of the multiferroic material equation (13). The spectrum is determined by the magnetization $\langle\sigma_M\rangle$, the polarization $\langle\sigma_P\rangle$, the anharmonic phonon interactions $\bar{B}_q, \bar{A}_q$ as well as the various spin-phonon coupling parameters $\bar{R}^{(m)}$ and $\bar{R}^{(f)}$. In this section the results will be discussed and compared with experimental observations. Depending on the sign of the spin-phonon interaction constant $R$ (see Eq. (7)), the phonon frequencies become either harder or softer. Which situation is actually realized depends on the interaction between the ferroic subsystems and hence it is a material-specific property. In $BiMnO_3$ and $YCrO_3$ one observes an interaction between the ferromagnetic and the ferroelectric subsystem, whereas $YMnO_3$ and $BiFeO_3$ offer a

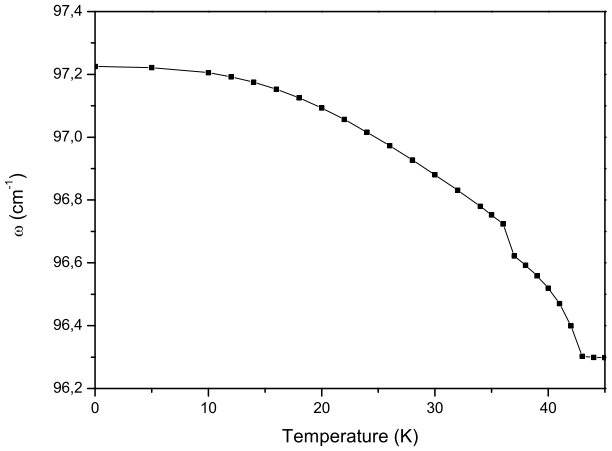



**Fig. 2.** Temperature dependence of the phonon energy for $TbMn_2O_5$ with $K_0 = -7$ K, $R_0^{(m)} = -0.35$ cm$^{-1}$, $R_0^{(f)} = -0.45$ cm$^{-1}$, $F_0^{(m)} = F_0^{(f)} = 4$ cm$^{-1}$. The bare phonon frequency is $\omega_0 = 96.3$ cm$^{-1}$. The mode shows a softening behavior for negative spin-phonon coupling $R$.

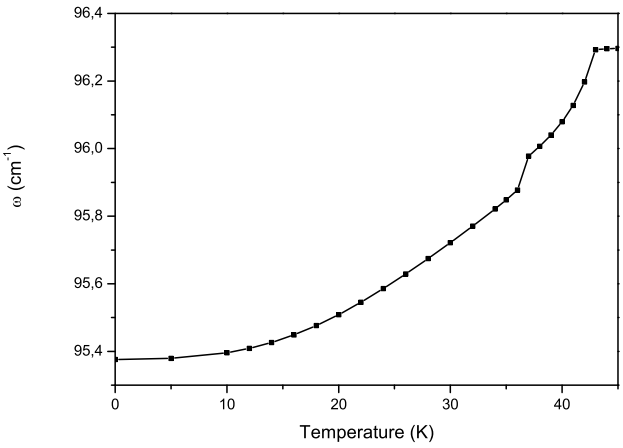



**Fig. 3.** Temperature dependence of the phonon energy for $TbMn_2O_5$ with $K_0 = -7$ K, $R_0^{(m)} = 0.70$ cm$^{-1}$, $R_0^{(f)} = 0.90$ cm$^{-1}$, $F_0^{(m)} = F_0^{(f)} = 4$ cm$^{-1}$. The mode offers hardening for positive spin-phonon coupling $R$.

coupling between an antiferromagnetic and ferroelectric systems [1]. As demonstrated in reference [36] $BiCrO_3$ films again exhibit a multiferroic coupling between antiferroelectricity and antiferromagnetism (or weak ferromagnetism). Hexagonal $YMnO_3$ shows likewise a coupling between ferroelectric and magnetic ordering [37]. The measured temperature dependence of the phonon mode in $TbMn_2O_5$ reveals a softening of that mode [4] which suggests a negative coupling parameter $R < 0$. In the opposite case $R > 0$ the phonon mode becomes harder. Following this line we have analyzed the influence of the magnetic and the ferroelectric subsystem as well as the ME coupling on the phonon excitation energy. In particular, let us emphasize the anomalies around the ferroelectric and magnetic phase transitions. The numerical calculations for the optical phonon energy is based on the following model parameters which are relevant for $TbMn_2O_5$: $T_C = 37$ K, $T_N = 43$ K, $J_0' = 75$ K, $K_0 = -7$ K, $s = 1/2$, $S = 2$, $\omega_0 = 96.3$ cm$^{-1}$. The anharmonic interaction parameters are estimated to be $A = -1$ cm$^{-1}$, $B = 0.5$ cm$^{-1}$, $F_0^{(m)} = F_0^{(f)} = 4$ cm$^{-1}$. Notice, that we have used the unit K (Kelvin) for all energy-related quantities, i.e. the Boltzmann constant $k_B$ is set to 1. As mentioned above the spin-phonon interaction constant $R$ can be positive or negative leading to hardening or softening of the phonon mode, respectively. The experimental data presented for $TbMn_2O_5$ show a softening of the phonon mode which is consistent with $R < 0$. A softening of the phonon mode at zero-wave vector $\omega(q = 0, T)$ with increasing temperature is also observed for $DyMn_2O_5$, $BiMn_2O_5$ [12] and $EuMn_2O_5$ [13]. The frequency of the mode versus the temperature is shown in Figure 2. The harmonic phonon energy $\omega_0$ introduced in equation (3) is renormalized due to the anharmonic spin-phonon and phonon-phonon interaction terms and becomes temperature dependent. The phonon excitation is obtained in equation (13). The spin-phonon interactions are dominant at low temperatures, whereas at higher temperatures, above $T_N$, there remains only the anharmonic phonon-phonon coupling. Totally the phonon energy decreases slightly. The dispersion relation in Figure 2 shows two kinks at the ferroelectric phase transition temperature $T_C = 37$ K and at the magnetic transition $T_N = 43$ K. The first anomaly occurs when the ferroelectric order disappears. As above $T_C$ the ME coupling $K_0$ is irrelevant, the kink in the dispersion relation is a direct consequence of the ME coupling. The second kink reflects the influence of the magnetic order on the phonon energy. The frequency shift below $T_C$ is mainly originated by the anharmonic spin-phonon interactions introduced in equation (7). Let us remind that the spin-phonon coupling comes from the exchange interaction $J_{ij} = J(r_i - r_j)$ (and $\tilde{J}_{ij}$, compare Eq. (2), as well as $J'_{ij}$, see Eq. (3)). Assuming the interaction depends on the actual lattice coordinates they can be expanded with respect to the phonon displacements $u_i$ and $u_j$. Hence the spin-phonon coupling parameters are determined by the first and second order derivatives of the related exchange coupling $J_{ij}$. The results shown in Figure 2 are in agreement with experimental observations in different $RMn_2O_5$ compounds [10–15]. In $TbMn_2O_5$ a small increase will be observed in the phonon curve between $T_C$ and $T_N$ [11]. Such a behavior can be reproduced in our approach if a positive coupling $R^{(m)} > 0$ is assumed within the temperature interval $T_C \leq T \leq T_N$. A hardening of the phonon mode is reported in $HoMn_2O_5$ [10], which is consistent with our studies adopting positive spin-phonon couplings $R^{(f)} > 0$ and $R^{(m)} > 0$ (see Fig. 3). The mentioned anomalies at $T_C$ and $T_N$ are also reproduced. Let us make a technical remark. Although the geometry of the lattice of $RMn_2O_5$ is quite complex, we have used a bcc structure for simplicity. The reason is that in our approach the geometrical structure is primarily included by the wave vector dependence of the coupling parameter. Moreover numerical simulations indicate the results will be not changed drastically using an orthorhombic structure.

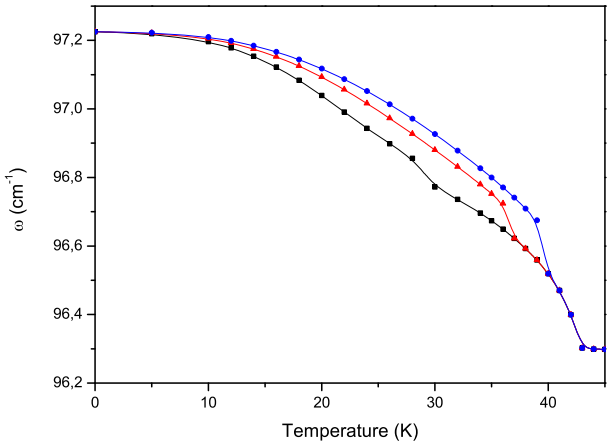
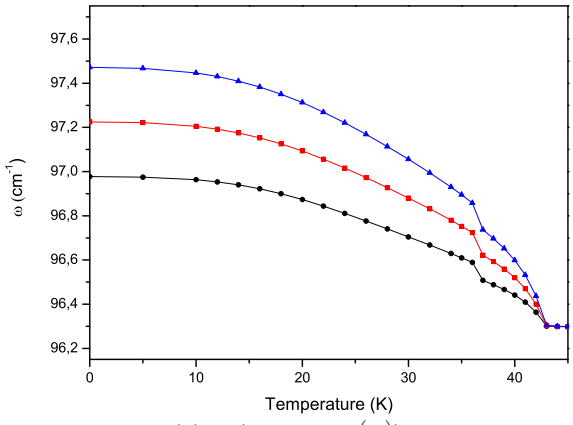



**Fig. 4.** Temperature dependence of the phonon energy for different magnetoelectric coupling $K_0 = -3$ K (black/lower curve); $K_0 = -7$ K (red/middle curve); $K_0 = -10$ K (blue/upper curve).

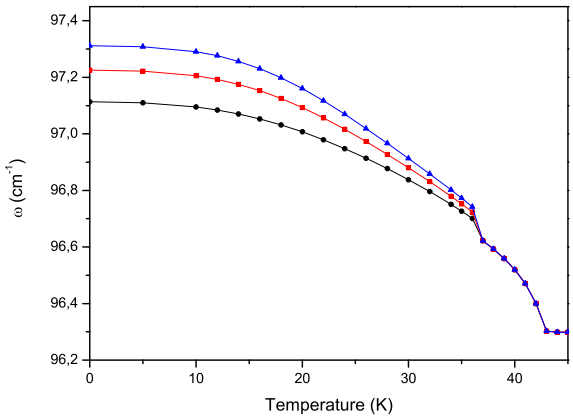
The ME coupling parameter is introduced in equation (6). The effect of the magnetoelectric coupling constant $K_0$ between the magnetic and electric subsystems is shown in Figure 4. As shown, the phonon energy depends on the ME coupling $K_0$ in a significant manner. The kink at $T_C$ is shifted to higher temperatures, i.e. $T_C$ is increased for stronger ME coupling. The magnetic phase transition temperature $T_N$ remains unchanged by the ME coupling $K_0$ [38]. There is also an experimental evidence for different coupling strengths and even for different coupling mechanisms between the magnetic and the ferroelectric subsystems. So the replacement of Y atoms by magnetic Ho atoms in $YMnO_3$ leads to a stronger suppression of the thermal conductivity [39]. Another study in reference [40] predicts that the polarization in orthorhombic $HoMnO_3$ with biquadratic ME coupling would be enhanced by up to two orders of magnitude with respect to that in orthorhombic $TbMnO_3$. In that compound the ME interaction term is linear in the electrical dipole moments.

The phonon energy is very sensitive to the anharmonic spin-phonon interaction constants $R^{(m)}$ and $R^{(f)}$. The situation is depicted in Figure 5. The phonon energy increases strongly with increasing $R^{(m)}$ below $T_N$ (see Fig. 5a), or with $R^{(f)}$ below $T_C$, in the multiferroic phase, compare Figure 5b. Synchrotron X-ray studies give some evidence of lattice modulation in the ferroelectric phase of $YMn_2O_5$ [41], however the atomic displacements seem to be extremely small. Moreover, several phonons in $TbMn_2O_5$ exhibit explicit correlations to the ferroelectric properties of these materials [11].

Until now the calculations are performed for zero external fields. However the magnetization and polarization in multiferroic substances are affected by such external electric or magnetic fields. The influence of an external magnetic field $h = g\mu_B B$ (see Eq. (2)), on the polarization $P$ is demonstrated experimentally in $TmMn_2O_5$ [42], in $MnWO_4$ [43] and in orthorhombic $YMnO_3$ [44]. The strong ME coupling in these materials can be illustrated by studying the influence of an applied magnetic field




(a) $\omega(q = 0, T, R^{(m)})$




(b) $\omega(q = 0, T, R^{(f)})$

**Fig. 5.** Temperature dependence of the phonon energy for different magnetic spin-phonon couplings: magnetoelectric couplings: (a): $R^{(m)} = -0.45$ K (black/lower curve); $R^{(m)} = -0.70$ K (red/middle curve); $R^{(m)} = -0.95$ K (blue/upper curve); (b): $R^{(f)} = -0.45$ K (black/lower curve); $R^{(f)} = -0.90$ K (red/middle curve); $R^{(f)} = -1.95$ K (blue/upper curve).

on the phonon spectrum. The result of our calculation is shown in Figure 6. The phonon energy $\omega$ increases with increasing magnetic field $h$. Significant changes of the phonon energy due to magnetic fields are reported for orthorhombic $TbMnO_3$ [45] and for hexagonal $HoMnO_3$ [46]. Unfortunately experimental data for $RMn_2O_5$ are still missing. Both phase transitions are indicated by the corresponding kinks in the phonon energy. For higher temperatures beyond 45 K we find no peculiarities. Figure 6 shows that under the influence of a magnetic field the phase transition temperatures $T_C$ and $T_N$ are altered, where the effect is more pronounced for $T_C$ as a further indication of the magnetoelectric behavior. So the phase transition temperature $T_C$ is enhanced by about 4–5 K. These changes are very sensitive to the model parameters. The increase of $T_C$ with the magnetic field $h$ and a vanishing kink at $T_N$ is observed in reference [47]. The dependence of the phonon frequency on the magnetic field is depicted in Figure 7. As expected the phonon excitation

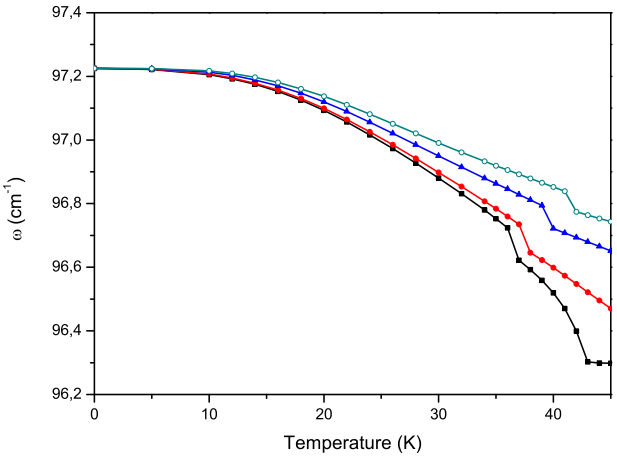



**Fig. 6.** Phonon energy versus temperature for different external magnetic field: $h = 0$ (black/lower curve), $h = 1$ K (read curve), $h = 5$ K (blue curve), $h = 10$ K (green curve).

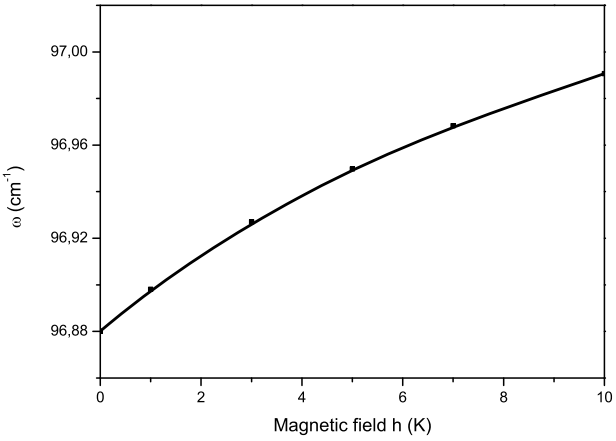



**Fig. 7.** Phonon frequency versus the magnetic field at fixed temperature, $T = 30$ K.

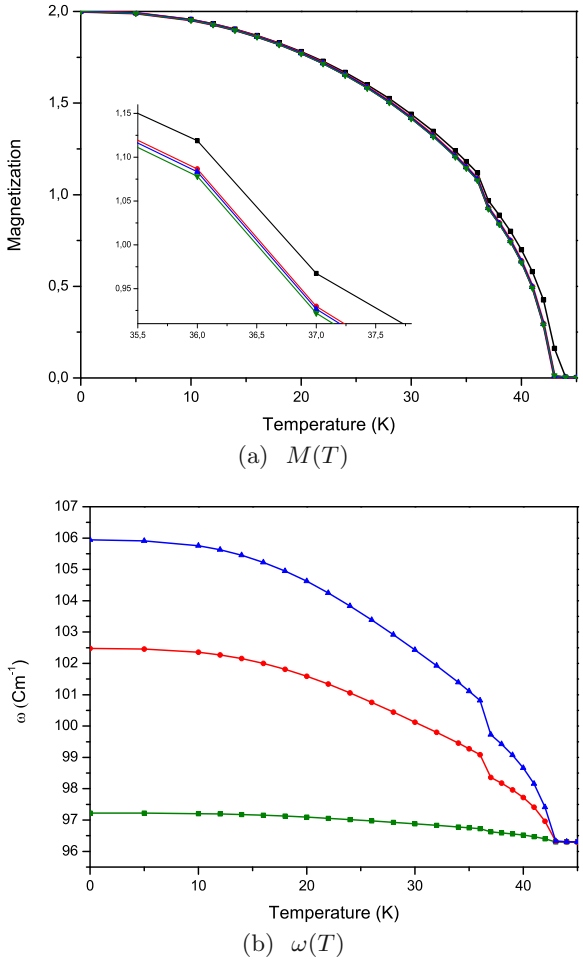



**Fig. 8.** Temperature dependence of the (a) magnetization and (b) the phonon energy for changed spin-phonon coupling: $R^{(m)} = 0.95$ cm$^{-1}$ (blue), $R^{(m)} = 0.70$ cm$^{-1}$ (red), $R^{(m)} = 0.70$ cm$^{-1}$ (green).

energy for wave vector $\vec{q} =$ is enhanced when the field is increased. As remarked in reference [48] the effect of a magnetic field or hydrostatic pressure are strongly dependent on the $R$ atom in the $R\mathrm{Mn_2O_5}$ systems. The compression of these materials is supposed to be equivalent to applying a magnetic field [49]. In references [9,50] it has been shown that the coupling between the magnetic orders and the dielectric properties in multiferroic $R\mathrm{Mn_2O_5}$ ($R$ = Ho, Dy, Tb) is mediated by the lattice distortion. The mentioned compounds have different ionic sizes. Hence the thermal expansion data display specific differences of the lattice strains. In case $R$ stands for Ho and Dy then a contraction appears along the $c$-axis, while one observes an expansion along the $a$- and $b$-axis at $T_C$. The opposite behavior is observed for Tb. The origin of this fact is due to the different spin modulations along the $c$-axis. The spin-lattice coupling leads to different stress in the lattice.

As demonstrated in the previous section, the Green's function technique allows also to calculate macroscopic quantities like the magnetization $M = \langle \sigma_M \rangle$ and the influence of the phonon degrees of freedom on $M$. The results are shown in Figure 8. In Figure 8a one finds the influence of the spin-phonon coupling on the magnetization $M(T)$. Increasing the spin-phonon coupling parameter $R^{(m)}$ the magnetization decreases. As expected then the magnetic transition temperature $T_N$ is lowered. In Figure 8b the phonon energy is represented as function of the temperature with different spin-phonon couplings. The phonon excitation energy increases strongly when the spin-phonon coupling $R^{(m)}$ is enhanced. In the same manner the magnetization is slightly decreased. Obviously the lattice degrees of freedom affect the magnetization and the phonon spectrum. Thus, for rare-earth $R = Tb$ the system offers a tensile strain. The ordered Mn magnetic moments are suppressed at high pressure. The kink at $T_C$ is due to the ME coupling and can be observed again. Our results are in agreement with the experimental data for orthorhombic $\mathrm{BiMnO_3}$ and $\mathrm{LuFe_2O_4}$ [51,52]. There are no data available for the influence of pressure on the magnetic properties of MF $R\mathrm{Mn_2O_5}$ systems. For the polarization the influence of the coupling is not very pronounced.

The effect is clearly stronger for the magnetization than for the polarization.

## 4 Conclusion

By using a realistic quantum model we have studied the multiferroic phases in $R\mathrm{Mn_2O_5}$ focusing on crucial roles of the phonon spectrum. The ferroelectric subsystem is characterized by both displacive-like couplings manifested by lattice distortions and order-disorder-like elements expressed in terms of pseudo-spins. The magnetic subsystem comprises the nearest neighbor ferromagnetic coupling and next nearest neighbor antiferromagnetic interaction. The interplay between these two couplings leads to collinear magnetic structures. As the consequence of the detailed characterization of both subsystems the coupling between the ferroic phases is not only given by a direct magnetoelectric coupling but additionally by spin-phonon couplings. To be specific we have introduced two kinds of spin-phonon couplings, namely the magnetic dominated ones, $R^{(m)}, F^{(m)}$ and the ferroelectric dominated ones characterized by the parameters $R^{(f)}, F^{(f)}$. The system undergoes a magnetic phase transition at the temperature $T_N$ with a finite sublattice magnetization. A further lowering of the temperature offers a second phase transition at $T_C < T_N$, below that the system develops a ferroelectric phase with a nonzero polarization. The paper is focused on the influence of the various couplings on the phonon spectrum of the multiferroic system. Such collective properties can be elucidated by a Green's function technique. Due to the magnetoelectric coupling the harmonic phonon mode is renormalized and becomes temperature dependent. The effect is the stronger the higher the magnetoelectric coupling is. Both phase transitions are manifested by a kink in the phonon spectrum at the corresponding transition temperatures. The behavior of the modified phonon mode is strongly influenced by the spin-phonon coupling. For positive couplings the mode becomes harder whereas for negative coupling the mode becomes softer. In the latter case we show that the phonon spectrum is very sensitive to a change of the magnetic spin-phonon coupling, while for different couplings the kink in the dispersion relation is maintained. In the same manner the ferroelectric pseudo-spin-phonon coupling, relevant for $T < T_C$, alters the phonon spectrum. The phonon mode can be also influenced by an external magnetic field, i.e. the phonon frequency can be triggered by a magnetic field. The Green's function method allows to figure out the behavior of macroscopic quantities as magnetization or polarization. We show that the magnetization is influenced by the spin-phonon coupling in such a manner that an increase of the coupling leads to a decrease of the magnetization.

One of us (S.G.B.) acknowledges support by the International Max Planck Research School for Science and Technology of Nanostructures in Halle. J.M.W. is also indebted to the Max Planck Institute of Microstructure Physics in Halle for financial support.

## Appendix A: Green's functions for the Ising model in a transverse field

The Hamiltonian of the ferroelectric subsystem and magnetoelectric coupling reads after rotation

$$\begin{aligned} H_{\mathrm{tim}} + H_{\mathrm{mf}} = &-\Omega \sum_i \left[ (1-2\rho_i)\sin\nu + \left(b_i^\dagger + b_i\right)\cos\nu) \right] \\ &- \frac{1}{8}\sum_{i,j} J'_{i,j} \Big( \left(b_i^\dagger b_j^\dagger + b_i^\dagger b_j + b_i b_j^\dagger + b_i b_j\right) \\ &\times \sin^2\nu - \left(b_j^\dagger + b_j - 2\rho_i b_j^\dagger - 2\rho_i b_j\right) \\ &\times \sin\nu\cos\nu - \left(b_i^\dagger + b_i - 2b_i^\dagger\rho_j - b_i\rho_j\right) \\ &\times \sin\nu\cos\nu + (1-2\rho_j - 2\rho_i + 4\rho_i\rho_j)\cos^2\nu \Big) \\ &+ \frac{1}{2}\sum_{i,j} K_{ij} S_i^z S_j^z \cos\nu - \sum_{i,j,l} K_{ijl}\rho_i S_j^z S_l^z \cos\nu \\ &- \frac{1}{2}\sum_{i,j,l} K_{ijl}\left(b_i^\dagger + b_i\right) S_j^z S_l^z \sin\nu. \end{aligned} \tag{A.1}$$

The matrix Green's function obeys

$$\begin{aligned} \begin{pmatrix} G_q^{f11} & G_q^{f12} \\ G_q^{f21} & G_q^{f22} \end{pmatrix} = &\begin{pmatrix} 2\langle\sigma_P\rangle & 0 \\ 0 & -2\langle\sigma_P\rangle \end{pmatrix} \\ &+ \begin{pmatrix} {\varepsilon_q}^{11} & {\varepsilon_q}^{12} \\ {\varepsilon_q}^{21} & {\varepsilon_q}^{22} \end{pmatrix} \begin{pmatrix} G_q^{f11} & G_q^{f12} \\ G_q^{f21} & G_q^{f22} \end{pmatrix}, \end{aligned}$$

with

$$\begin{aligned} {\varepsilon_q}^{11} &= 2\Omega\sin\nu + J'_0\langle\sigma_P\rangle\cos^2\nu \\ &\quad - K_0\cos\nu\langle\sigma_M\rangle^2 - \frac{1}{2}J'_q\langle\sigma_P\rangle\sin^2\nu \\ &\quad + F^{(f)}\langle Q\rangle\cos\nu + \frac{1}{2}R^{(f)}\langle Q^2\rangle\cos\nu \\ {\varepsilon_q}^{12} &= -\frac{1}{2}J'_q\langle\sigma_P\rangle\sin^2\nu \\ {\varepsilon_q}^{21} &= -{\varepsilon_q}^{12} \quad {\varepsilon_q}^{22} = -{\varepsilon_q}^{11}. \end{aligned} \tag{A.2}$$

The solution for the Green's functions are

$$\begin{aligned} G_q^{f11} &= \frac{\langle\sigma_P\rangle\left[E + {\varepsilon_q}^{11}\right]}{\left(E - {\varepsilon_q}^{11}\right)\left(E + {\varepsilon_q}^{11}\right) + \left({\varepsilon_q}^{12}\right)^2} \\ G_q^{f12} &= \frac{\langle\sigma_P\rangle{\varepsilon_q}^{12}}{\left(E - {\varepsilon_q}^{11}\right)\left(E + {\varepsilon_q}^{11}\right) - \left({\varepsilon_q}^{12}\right)^2} \\ G_q^{f21} &= \frac{\langle\sigma_P\rangle{\varepsilon_q}^{12}}{\left(E - {\varepsilon_q}^{11}\right)\left(E + {\varepsilon_q}^{11}\right) - \left({\varepsilon_q}^{12}\right)^2} \\ G_q^{f22} &= -\frac{\langle\sigma_P\rangle\left[E - {\varepsilon_q}^{11}\right]}{\left(E - {\varepsilon_q}^{11}\right)\left(E + {\varepsilon_q}^{11}\right) - \left({\varepsilon_q}^{12}\right)^2}. \end{aligned} \tag{A.3}$$

The most relevant function $G^{f11}$ is given in the text as equation (10) where the coefficients are given by:

$$\epsilon_q = \frac{{\varepsilon_q}^{11}}{2E_{\rm f}(q)} + \frac{1}{2}, \quad \epsilon'_q = \frac{{\varepsilon_q}^{11}}{2E_{\rm f}(q)} - \frac{1}{2}. \tag{A.4}$$

Here, we have defined $E_{\rm f}(q) = \sqrt{({\varepsilon_q}^{11})^2 - ({\varepsilon_q}^{12})^2}$.

## Appendix B: Phonon Green's function

As mentioned in the text, the phonon Green's functions are also given by a matrix defined in equation (11)

$$\begin{pmatrix} \langle\langle a_q; a_q^\dagger\rangle\rangle & \langle\langle a_q; a_q\rangle\rangle \\ \langle\langle a_q^\dagger; a_q^\dagger\rangle\rangle & \langle\langle a_q^\dagger; a_q\rangle\rangle \end{pmatrix} \equiv \begin{pmatrix} G_q^{11} & G_q^{12} \\ G_q^{21} & G_q^{22} \end{pmatrix}. \tag{B.1}$$

These set fulfills the equation of motion given by equation (12) with the following coefficients:

$$\begin{aligned} {\varpi_q}^{11} &= \omega_q^0 + \bar{B}_q\langle Q\rangle + \frac{1}{2}\bar{A}_q\langle Q^2\rangle - \frac{1}{2}\bar{R}^{(m)}(q)\langle\sigma_M\rangle \\ &\quad - \frac{1}{2}\bar{R}^{(f)}(q)\langle\sigma_P\rangle\cos\nu \\ {\varpi_q}^{12} &= \bar{B}_q\langle Q\rangle + \frac{1}{2}\bar{A}_q\langle Q^2\rangle - \frac{1}{2}\bar{R}^{(m)}(q)\langle\sigma_M\rangle \\ &\quad - \frac{1}{2}\bar{R}^{(f)}(q)\langle\sigma_P\rangle\cos\nu \\ {\varpi_q}^{11} - {\varpi_q}^{12} &= \omega_q^0, \quad {\varpi_q}^{21} = -{\varpi_q}^{12}, \quad {\varpi_q}^{22} = -{\varpi_q}^{11}. \end{aligned} \tag{B.2}$$

Furthermore we have defined $\bar{B}(q) = B(q)/(2w_q^0)$ and $\bar{A}(q) = A(q)/(2w_q^0)$ and correspondingly $\bar{R}^{(m)}$ and $\bar{R}^{(f)}$. From here we conclude the phonon dispersion relation as:

$$\omega(q) = \sqrt{({\varpi_q}^{11})^2 - ({\varpi_q}^{12})^2}. \tag{B.3}$$

The final result is given in the text as equation (13).

## References


1. N.A. Hill, J. Phys. Chem. B **104**, 6694 (2000)
2. T. Kimura, S. Kawamoto, I. Yamada, M. Azuma, M. Takano, Y. Tokura, Phys. Rev. B **67**, 180401 (2003)
3. T. Kimura, T. Goto, H. Shintani, K. Ishizaka, T. Arima, Y. Tokura, Nature **426**, 55 (2003)
4. N. Hur, S. Park, P.A. Sharma, J. Ahn, S. Guha, S.-W. Cheong, Nature **429**, 392 (2004)
5. S.-W. Cheong, M. Mostovoy, Nat. Mater. **6**, 13 (2007)
6. D. Khomskii, Physics **2**, 20 (2009)
7. K.F. Wang, J.M. Liu, Z.F. Ren, Adv. Phys. **58**, 321 (2009)
8. C. Wang, G.-C. Guo, L. He, Phys. Rev. B **77**, 134113 (2008)
9. C.R. dela Cruz, R. Yen, B. Lorenz, S. Park, S.-W. Cheong, M.M. Gospodinov, W. Ratcliff, J.W. Lynn, C.W. Chu, J. Appl. Phys. **99**, 08R103 (2006)
10. B. Mihailova, M.M. Gospodinov, B. Güttler, F. Yen, A.P. Litvinchuk, M.N. Iliev, Phys. Rev. B **71**, 172301 (2005)
11. R. Valdés Aguilar, A.B. Sushkov, S. Park, S.-W. Cheong, H.D. Drew, Phys. Rev. B **74**, 184404 (2006)
12. A.F. Garcia-Flores, E. Granado, H. Martinho, R.R. Urbano, C. Rettori, E.I. Golovenchits, V.A. Sanina, S.B. Oseroff, S. Park, S.-W. Cheong, Phys. Rev. B **73**, 104411 (2006)
13. E. Garcia-Flores, A.F. Granado, H. Martinho, C. Rettori, E.I. Golovenchits, V.A. Sanina, S.B. Oseroff, S. Park, S.-W. Cheong, J. Appl. Phys. **101**, 09M106 (2007)
14. C.L. Lu, J. Fan, H.M. Liu, K. Xia, K.F. Wang, P.W. Wang, Q.Y. He, D.P. Yu, J.-M. Liu, Appl. Phys. A **96**, 991 (2009)
15. J. Cao, L.I. Vergara, J.L. Musfeldt, A.P. Litvinchuk, Y.J. Wang, S. Park, S.-W. Cheong, Phys. Rev. B **78**, 064307 (2008)
16. L. Martin-Carron, A. de Andres, M.J. Martinez-Lopez, M.T. Casais, J.A. Alonso, J. Alloys Compd. **323–324**, 494 (2001)
17. A.B. Sushkov, R.V. Aguilar, S. Park, S.-W. Cheong, H.D. Drew, Phys. Rev. Lett. **98**, 027202 (2007)
18. K. Cao, G.-C. Guo, L. He, J. Phys.: Condens. Matter **24**, 206001 (2012)
19. A.P. Litvinchuk, J. Magn. Magn. Mater. **321**, 2373 (2009)
20. C. Jia, J. Berakdar, Europhys. Lett. **85**, 57004 (2009)
21. C. Jia, J. Berakdar, Phys. Stat. Sol. B **247**, 662 (2010)
22. M. Mochizuki, N. Furukawa, N. Nagaosa, Phys. Rev. B **84**, 144409 (2011)
23. S. Kovachev, J.M. Wesselinowa, J. Phys.: Condens. Matter **22**, 255901 (2010)
24. R. Blinc, B. Žekš, Adv. Phys. **21**, 693 (1972)
25. H. Katsura, N. Nagaosa, A.V. Balatsky, Phys. Rev. Lett. **95**, 057205 (2005)
26. C. Jia, S. Onoda, N. Nagaosa, J.H. Han, Phys. Rev. B **74**, 224444 (2006)
27. L.C. Chapon, G.R. Blake, M.J. Gutmann, S. Park, N. Hur, P.G. Radaelli, S.-W. Cheong, Phys. Rev. Lett. **93**, 177402 (2004)
28. L.C. Chapon, P.G. Radaelli, G.R. Blake, S. Park, S.-W. Cheong, Phys. Rev. Lett. **96**, 097601 (2006)
29. G.R. Blake, L.C. Chapon, P.G. Radaelli, S. Park, N. Hur, S.-W. Cheong, J. Rodriguez-Carvajal, Phys. Rev. B **71**, 214402 (2005)
30. S.V. Tjablikov, *Methods in the Quantum Theory of Magnetism* (Plenum Press, New York, 1967)
31. J.-H. Kim, M.A. van der Vegte, A. Scaramucci, S. Artyukhin, J.-H. Chung, S. Park, S.-W. Cheong, M. Mostovoy, S.-H. Lee, Phys. Rev. Lett. **107**, 097401 (2011)
32. M. Mostovoy, A. Scaramucci, N.A. Spaldin, K.T. Delaney, Phys. Rev. Lett. **105**, 087202 (2010)
33. J.M. Wesselinowa, S. Kovachev, Phys. Rev. B **75**, 045411 (2007)
34. I. Apostolova, A.T. Apostolov, J.M. Wesselinowa, J. Phys.: Condens. Matter **21**, 036002 (2009)
35. W. Nolting, *Fundamentals of Many-body Physics* (Springer-Verlag, Berlin, 2009)
36. N. Lee, M. Varela, H.M. Christen, Appl. Phys. Lett. **89**, 162904 (2006)
37. Z.J. Huang, Y. Cao, Y.Y. Sun, Y.Y. Xue, C.W. Chu, Phys. Rev. B **56**, 2623 (1997)
38. S.G. Bahoosh, J.M. Wesselinowa, S. Trimper, submitted to J. Phys. D (2012)
39. P.A. Sharma, J.S. Ahn, N. Hur, S. Park, S.B. Kim, S. Lee, J.-G. Park, S. Guha, S.-W. Cheong, Phys. Rev. Lett. **93**, 177202 (2004)

40. I.A. Sergienko, C. Şen, E. Dagotto, Phys. Rev. Lett. **97**, 227204 (2006)
41. I. Kagomiya, S. Matsumoto, K. Kohn, Y. Fukuda, T. Shoubu, H. Kimura, Y. Noda, N. Ikeda, Ferroelectrics **286**, 167 (2003)
42. M. Fukunaga, Y. Sakamoto, H. Kimura, Y. Noda, N. Abe, K. Taniguchi, T. Arima, S. Wakimoto, M. Takeda, K. Kakurai, K. Kohn, Phys. Rev. Lett. **103**, 077204 (2009)
43. R.P. Chaudhury, B. Lorenz, Y.Q. Wang, Y.Y. Sun, C.W. Chu, Phys. Rev. B **77**, 104406 (2008)
44. I. Fina, L. Fabrega, X. Marti, F. Sanchez, J. Fontcuberta, Appl. Phys. Lett. **97**, 232905 (2010)
45. H. Barath, M. Kim, S.L. Cooper, P. Abbamonte, E. Fradkin, I. Mahns, M. Rübhausen, N. Aliouane, D.N. Argyriou, Phys. Rev. B **78**, 134407 (2008)
46. S.-W. Cheong, in *Proceedings of the international conference on Low Energy Electrodynamics in Solids, Tallinn, 2006*, p. 62
47. S.M. Feng, Y.S. Chai, J.L. Zhu, N. Manivannan, Y.S. Oh, L.J. Wang, Y.S. Yang, C.Q. Jin, K.H. Kim, New J. Phys. **12**, 0730006 (2010)
48. Y. Noda, H. Kimura, M. Fukunaga, S. Kobayashi, I. Kagomiya, K. Kohn, J. Phys.: Condens. Matter **20**, 434206 (2008)
49. C.R. dela Cruz, B. Lorenz, Y.Y. Sun, Y. Wang, S. Park, S.-W. Cheong, M.M. Gospodinov, C.W. Chu, Phys. Rev. B **76**, 174106 (2007)
50. C.R. dela Cruz, F. Yen, B. Lorenz, M.M. Gospodinov, C.W. Chu, W. Ratcliff, J.W. Lynn, S. Park, S.-W. Cheong, Phys. Rev. B **73**, 100406 (2006)
51. C.C. Chou, S. Taran, J.L. Her, C.P. Sun, C.L. Huang, H. Sakurai, A.A. Belik, E. Takayama-Muromachi, H.D. Yang, Phys. Rev. B **78**, 092404 (2008)
52. X. Shen, C.H. Xu, C.H. Li, Y. Zhang, Q. Zhao, H.X. Yang, Y. Sun, J.Q. Li, C.Q. Jin, R.C. Yu, Appl. Phys. Lett. **96**, 102909 (2010)